Analysis of quantization error in financial pricing via finite difference methods

Christina C. Christara and Nat Chun-Ho Leung

Department of Computer Science
University of Toronto
Toronto, Ontario M5S 3G4, Canada
{ccc,natleung}@cs.toronto.edu

Abstract

In this paper, we study the error of a second order finite difference scheme for the one-dimensional convection-diffusion equation. We consider non-smooth initial conditions commonly encountered in financial pricing applications. For these initial conditions, we establish the explicit expression of the *quantization error*, which is loosely defined as the error of the numerical solution due to the placement of the point of non-smoothness on the numerical grid. Based on our analysis, we study the issue of optimal placement of such non-smoothness points on the grid, and the effect of smoothing operators on quantization errors.

Key words: non-smooth initial conditions, option pricing, numerical solution, partial differential equation, convection-diffusion equations, Fourier analysis, finite difference methods, Black-Scholes equation, Greeks

1 Introduction

For many financial pricing problems, exact solutions based on elementary functions are often unknown, and numerical solutions to the Black-Scholes equation and its variants are required. For diffusion-based linear problems, under general assumptions one can expect the solution to be at least C^2 in the interior of the spatial domain and at least C^1 in time. In fact, for the problems we consider in this paper, the solutions are C^∞ in both space and time away from the initial time. Local analysis of leading error terms, common in numerical analysis textbooks, shows that, under sufficient smoothness assumptions that include the initial time, the Crank-Nicolson timestepping method combined with central differencing in space should yield second order convergence to the solution of the partial differential equation (PDE).

However, special difficulties arise in applying classical PDE timestepping methods to pricing European contracts whose payoffs are not smooth in space. The European call option with payoff given by $\max(S(T) - K, 0)$, considered as a function of the terminal asset price $S(T)$, does not have a continuous first derivative at the strike K. The non-smoothness is known to cause high frequency errors under a classical Crank-Nicolson time discretization [1].

The Rannacher timestepping method has been proposed [9] to address the difficulty with non-smooth initial data. In this method, the first few timesteps of the Crank-Nicolson timestepping are replaced by fully implicit timesteppings to restore optimal convergence order. It has been shown for various non-smooth initial conditions that the Rannacher start-up is able to suppress the high frequency error associated with the non-smoothness.

An analysis of the Crank-Nicolson-Rannacher timestepping for the Black-Scholes equation and finite difference methods is found in [1], while [17] extends the analysis to two-dimensional Black-Scholes and the alternating direction implicit modified Craig-Sneyd method. The detailed investigation in [1] considers Dirac delta initial conditions and decomposes the Crank-Nicolson-Rannacher timestepping operator in low-, mid- and high-frequency components, and shows that the error in the low-frequency component is more prominent. It also concludes that replacing each of the first two timesteps (of step-size k) with two timesteps of step-size $\frac{k}{2}$ is the optimal choice to reduce high-frequency errors associated with non-smoothness of the initial condition while not increasing the more prominent low-frequency errors. This is known as the *Crank-Nicolson-Rannacher* (CN-Rannacher) method.

Other implementations of the Rannacher timestepping, including replacing two initial Crank-Nicolson timesteps by two fully implicit timesteps, have been studied in [1]. We refer the reader to their work for these other possible choices.

Another novel timestepping technique has been proposed recently in [10], where it was shown that for Dirac-delta initial condition, a square root change of variable of the time dimension restores the optimal second order convergence (for small enough time-space step-size ratio) without the need of Rannacher timestepping. Numerical experiments there suggest that the technique is also useful for more complicated problems including the pricing of an American option. As an additional note, one could consider the use of the strongly A-stable second-order backward differentiation formula (BDF2) as an alternative to Crank-Nicolson to damp the high-frequency errors. However, it is noted in [16], that BDF2 performs poorly in the more complicated American options cases, such as shout options.

Convergence of difference schemes for non-smooth initial data has been studied theoretically in [12]. Smoothing schemes for such initial data, as a remedy to restore optimal convergence of difference schemes, are suggested in [5]. The study of Rannacher timestepping [9] is carried out with a finite element discretization, where the non-smooth initial condition is projected on the space of basis functions. This projection can be considered as a type of smoothing. In the most typical setting, the basis functions are piecewise linear, which means that, if there is a node at the discontinuity point, projection does not alter the call/put payoffs. In [11] mesh shifting techniques, mostly aligning the strike on a mid-point, are suggested to restore convergence order. Application of these approaches in the financial context can be found in [8], [4], [11] or [2]. In the course of our analysis, these approaches will also be discussed. In particular, in [8], three techniques for restoring the convergence order are studied: averaging the initial data, shifting the mesh and projecting the initial data on a space of basis functions. It is concluded through extensive numerical experiments that, for discontinuous payoffs, Rannacher timestepping must be accompagnied by one of the three techniques to obtain a stable second order convergence. Other regularization and smoothing techniques for the Dirac-delta and Heaviside functions can be found in [13], [14] or [15], among others.

This paper is dedicated to a detailed study of the leading error of the CN-Rannacher method due to grid resolution of the point of non-smoothness. We will focus on non-smoothness that is of most financial interest. In the course of the analysis, we will additionally develop and justify a few numerical schemes that could help achieve a stable convergence order. The contributions of the paper are:

- We develop a general framework to analyze the quantization error for a finite difference scheme in relation to the relative position of the non-smoothness in the grid. We consider an arbitrary relative positioning, α, of the point of non-smoothness in the grid, to be explicitly defined later. We derive explicit formulae for the leading terms of the quantization error for various types of non-smooth initial conditions, such as Dirac delta, Heaviside, ramp, and exponential ramp.
- We demonstrate that, in the presence of discontinuity/non-smoothness, the leading error of our finite difference solution depends not only on the spatial and time stepsizes, but also on α. We show that, for CN-Rannacher method with central differencing, the (more prominent) low-frequency error, derived in [1], can be (further) decomposed into a "normal" timestepping error component and a quantization error component, and it is the latter that is relevant to the positioning of the non-smoothness on the grid. In our model problem, the quantization error and its derivatives consists of a Gaussian centered at the point of non-smoothness.

- We demonstrate that, while the CN-Rannacher method is formally second order, for our finite difference scheme, suboptimal convergence can result from the placement of a discontinuity. While the result is known (see, for example, [8]), the result comes as a natural consequence of our mathematical analysis. In addition, our analysis shows that for the unsmoothed Heaviside initial condition, our finite difference solution has a first order quantization error proportional to $(\alpha - \frac{1}{2})$, explaining the inverse relationship between the error and the distance of the discontinuity from a mid-point in the grid. This explains the effect of mesh shifting techniques placing the discontinuity of the Heaviside function at mid-points noted experimentally in [8].
- Our analysis shows that an unstable convergence estimate can result when the relative position of the non-smoothness, α, is not maintained during grid refinement. We also studied the possibility of choosing an optimal α. For our choice of finite difference with an unsmoothed ramp (call or put) initial condition, the quantization error is second order with a $(\alpha^2 + \alpha - \frac{1}{6})$ coefficient, which gives two α values that result in minimum quantization error. This explains the numerical results in [7], in which, for the ramp function, the authors discovered two disjoint optimal ranges of α which contain the two roots of the quadratic function representing the quantization error. We also give a numerical example where a good choice of α could lead to third order convergence even though our numerical scheme of choice is only formally second order.
- Our analysis shows that quantization error in the solution propagates to its divided-difference-based derivatives, in the same form. In a financial setting, these derivatives (a.k.a. as Greeks) are important parameters for determining hedging strategies. Numerical errors due to mesh positioning could therefore have an undesirable impact on hedging.
- We demonstrate explicitly that smoothing operators can recover optimal convergence, which was a known result proved in a more general setting in [5]. While retaining $O(h^2)$ error by smoothing was known, our contribution lies in illustrating how and in which cases of initial conditions the dependence of the leading error on α can be removed by smoothing. From this, we derive in which cases maintaining α and applying smoothing can be used alternatively or must be used simultaneously to obtain second order convergence and stable order of convergence.

The outline of the remainder of the paper is as follows. In Section 2, we present numerical experiments that motivate our study, and define the model problem that we will study in this paper. In Section 3, we develop the analysis and obtain explicit leading error formulae, starting from a review of the techniques in [1]. In Section 4, we discuss the possibility of choosing an optimal positioning of the point of non-smoothness in the grid, and present corresponding experiments. In Section 5, we show how to obtain explicit leading error formulae for the Greeks. In Section 6, the effect of smoothing operators on the quantization error is discussed. Section 7 concludes.

2 Model problem

2.1 Non-smooth initial data and convergence

The Black-Scholes equation is one of the most important equations in financial pricing. In its basic form, the Black-Scholes equation is

$$\frac{\partial V}{\partial t} + \frac{\sigma^2 S^2}{2}\frac{\partial^2 V}{\partial S^2} + (r-q)S\frac{\partial V}{\partial S} - rV = 0, \tag{2.1}$$

where $V(t, S)$ is the value of the option at time t and asset price S, which is assumed to have continuous dividend rate q. The risk-free rate is assumed to be a constant r. The volatility σ is unobservable, and in the original formulation of the Black-Scholes model, this quantity is assumed to be a known constant. When this quantity is deterministically dependent on time and space, the resulting model is the local volatility model due to Dupire [3].

Upon substitution $x = \log(S)$ and $\tau = T - t$, equation (2.1) is transformed to a convection-diffusion equation with constant coefficients

$$\frac{\partial v}{\partial \tau} = \frac{\sigma^2}{2}\frac{\partial^2 v}{\partial x^2} + (r - q - \frac{\sigma^2}{2})\frac{\partial v}{\partial x} - rv, \tag{2.2}$$

where $v(\tau, x) = V(T - \tau, e^x)$.

The payoff of the option $g(S_T)$ dependent on the terminal asset price at maturity T translates into a terminal condition for (2.1) or an initial condition for (2.2). Numerical solutions to (2.1), (2.2) and their generalizations are important in many occasions. When more complex structures are specified, for example a parametric form of the local volatility or higher dimensional volatility models, exact solution based on elementary functions is often unknown even for basic payoff functions $g(\cdot)$. Numerical solutions to these equations therefore remain important for many applications.

Many financial derivatives, however, have non-smooth payoff functions. The most representative of all are the calls and puts, which respectively have the form $\max(S - K, 0)$ and $\max(K - S, 0)$, where K is known as the *strike*. The first derivative with respect to S is not continuous precisely at the strike $S = K$. Another common payoff that has similar difficulties is the digital option, which has payoff $\mathcal{H}(S - K)$ (or alternatively, $\mathcal{H}(K - S)$), where $\mathcal{H}(x) = \begin{cases} 1 & \text{if } x \geq 0 \\ 0 & \text{else} \end{cases}$ is the Heaviside function. This option pays off a fixed amount if and only if the asset price is above (or alternatively, below) a certain strike $S = K$. The payoff itself is not continuous at the strike.

It has been widely reported and known that applying a finite difference method with Crank-Nicolson directly to (2.1) or (2.2) with non-smooth initial data will result in erratic convergence rates and in some cases large errors in derivative approximations. The Rannacher timestepping successfully eliminates higher frequency errors and restores second order leading errors for calls and puts [1]. However, suboptimal convergence is still observed experimentally for digital options [8].

As an example, we consider solving (2.2) with an initial condition equal to $\mathcal{H}(x)$ so that discontinuity occurs at the strike $x = 0$. Equivalently, this is the price of a digital option that pays \$1 when $\exp(x)$ is above 1, under the assumption of geometric Brownian motion. We use a finite difference method with central differences and Rannacher timestepping, so that the first two Crank-Nicolson timesteps are replaced by four fully implicit timesteps of half the step-size. We begin with a uniform grid on $[-8, 8]$ with step-size $h = \frac{1}{12}$. For each successive run, we insert mid-points into the grid so that the grid remains uniform, and the step-size is halved. In this way, the discontinuity falls always at a grid-point. This is a common method of refining grids (but by no means the only one). We shall revisit this point later in the paper. Finally, Dirichlet conditions with the exact solution are imposed on the two far end-points. From the $(l-1)$-th mesh (coarser) to the l-th mesh (finer), we also define the quantity for $l > 1$:

$$\Upsilon_l \equiv \log\left(\left|\frac{\text{error}_{l-1}}{\text{error}_l}\right|\right) / \log(2).$$

The error is defined to be the numerical approximation minus the exact value of the solution to the PDE, at $t = 0$ (terminal point $\tau = T$). If the numerical scheme has first order convergence, then the error is approximately halved as the grid is refined by one level. In this case, the Υ_l's would be close to 1. On the other hand, one can expect the Υ_l's to be close to 2 for a quadratically convergent scheme.

The results from solving (2.2) with an initial condition equal to $\mathcal{H}(x)$ *using central difference with Rannacher timestepping* are shown in Table 2.1. It is evident that, in this setting, one only observes a

Spatial step-size h	Time step-size k	Error	Convergence rate estimate Υ
1/12	1/6	7.9320×10^{-2}	–
1/24	1/12	3.9038×10^{-2}	1.0228
1/48	1/24	1.9495×10^{-2}	1.0018
1/96	1/48	9.7551×10^{-3}	0.9989

Table 2.1: Results of solving equation (2.2) with initial condition the Heaviside function $\mathcal{H}(x)$. Solution evaluated at $x = 0$. Volatility σ is 20%, risk-free rate r is 5%, dividend q is 0% and maturity T is 1. Numerical method is Rannacher timestepping with central spatial difference. Each grid is refined by inserting mid-points. Discontinuity aligned with a grid-point.

Spatial step-size h	Time step-size k	Error	Convergence rate estimate Υ
1/12	1/6	1.6067×10^{-2}	–
1/24	1/12	2.3803×10^{-2}	-0.5670
1/48	1/24	3.9294×10^{-3}	2.5988
1/96	1/48	5.8572×10^{-3}	-0.5759

Table 2.2: Results of solving equation (2.2) with initial condition the Heaviside function $\mathcal{H}(x)$. Solution evaluated at $x = 0$. Volatility σ is 20%, risk-free rate r is 5%, dividend q is 0% and maturity T is 1. Numerical method is Rannacher timestepping with central spatial difference. Each grid is refined by inserting mid-points. Discontinuity not aligned with a grid-point. Cubic spline interpolation is used for the evaluation.

first order convergence experimentally. An existing technique in mitigating this sub-optimal convergence is by placing the discontinuity at a mid-point (e.g. [8]). We will revisit this technique from a different viewpoint as we develop the analysis later in the paper.

If the discontinuity is not a grid-point, which is a common scenario, and no additional effort is taken to align the discontinuity to a grid-point in the numerical software, then an erratic experimental convergence using the aforementioned way of refining grids might be observed. This can be seen in Table 2.2. In this experiment, the first grid has grid-points $(\frac{1}{30} + \frac{j}{12})$, $j = -100, \ldots, 92$, so that the endpoints are $(-8.3, 7.7)$, on which we impose Dirichlet boundary conditions based on the known exact solution. We refine the grid by inserting mid-points. In this way, the relative position of the strike 0 (which is the point of discontinuity) in the grid does not align with a grid-point but fluctuates. To carry the evaluation at the strike 0, cubic spline interpolation is used. As evident in Table 2.2, the error does not necessarily improve even as the step-sizes are halved. The experimental convergence is far from stable.

An erratic convergence could be problematic. Extrapolation, for example, is a common technique to eliminate the leading error term in order to obtain a more accurate solution using numerical solutions from a coarse grid and a finer grid. This is a useful technique when computational costs are high, for instance in a higher dimension PDE solver. However, extrapolation is only possible when the convergence is stable. It is difficult to obtain a reliable extrapolated value when the convergence is unstable, like the one in Table 2.2. The difficulty of extrapolation when convergence is unstable is also noted in [4].

Finally, the errors in Table 2.2 in fact are smaller than those in Table 2.1. This is an expected phenomenon and we will explain why placing the strike on a grid-point will lead to larger errors later in the paper.

The error resulting from the alignment of the non-smoothness is known as the *quantization error* in [11]. In other words, this is an error that arises from the resolution of the discontinuity (or point of non-smoothness) on the grid, on top of the classical finite difference discretization errors. In this paper, we will analyze in detail how this quantization error affects the quality of a numerical solution.

2.2 The convection-diffusion equation

As the logarithmic transformation converts the Black-Scholes equation to a convection-diffusion equation with constant coefficients, we work with the following model problem as in [1]:

$$\frac{\partial v}{\partial t} + a\frac{\partial v}{\partial x} = \frac{\partial^2 v}{\partial x^2}, \quad (t,x) \in (0,1] \times (-\infty,\infty). \tag{2.3}$$

We consider a finite difference method using second order central difference with Rannacher timestepping. Let h be the stepsize of a spatial discretization, and k be the time stepsize. Denote $t_l = lk$ (with $l = 1, 2, \ldots, m$ and $t_m = 1$) and $x_j = (j + (1-\alpha))h$, where $j \in \{\ldots, -1, 0, 1, \ldots\} = \mathbf{Z}$, and $\alpha \in (0,1]$. Let $v^{(l)}$ be a discrete approximation to v, i.e. $v_j^{(l)} \approx v(t_l, x_j)$. The fully implicit discretization of (2.3) with a time step-size of $\frac{k}{2}$ is

$$\frac{v_j^{(l)} - v_j^{(l-1)}}{\frac{k}{2}} = \frac{v_{j+1}^{(l)} - 2v_j^{(l)} + v_{j-1}^{(l)}}{h^2} - a\frac{v_{j+1}^{(l)} - v_{j-1}^{(l)}}{2h}, \tag{2.4}$$

whereas the Crank-Nicolson discretization of (2.3) with a time step-size k is as follows:

$$\begin{aligned}\frac{v_j^{(l)} - v_j^{(l-1)}}{k} &= \frac{1}{2}\Bigg(\frac{v_{j+1}^{(l-1)} - 2v_j^{(l-1)} + v_{j-1}^{(l-1)}}{h^2} - a\frac{v_{j+1}^{(l-1)} - v_{j-1}^{(l-1)}}{2h} \\ &\quad + \frac{v_{j+1}^{(l)} - 2v_j^{(l)} + v_{j-1}^{(l)}}{h^2} - a\frac{v_{j+1}^{(l)} - v_{j-1}^{(l)}}{2h}\Bigg).\end{aligned} \tag{2.5}$$

Our goal is to compare $v^{(m)}$ and $v(1,\cdot)$ and investigate the effect of non-smoothness on their discrepancy. We will also investigate how the error changes as we refine the grid by inserting mid-points into the previous mesh. As in Section 2.1, the quantity $\lambda = \frac{k}{h}$ is held constant as the grid is refined.

2.3 Difference equation and the discrete-time Fourier transform

For the rest of this paper, the variable i denotes the canonical choice of the complex number such that $i^2 = -1$. Following [1], for a function U defined on the discretized grid such that its value at x_j is given by U_j, we define the transform

$$\hat{U}(\theta) = h \sum_{j=-\infty}^{\infty} U_j e^{-\frac{ix_j\theta}{h}}. \tag{2.6}$$

The inverse transform is given by

$$U_j = \frac{1}{2\pi h}\int_{-\pi}^{\pi} \hat{U}(\theta) e^{\frac{ix_j\theta}{h}} d\theta = \frac{1}{2\pi}\int_{-\frac{\pi}{h}}^{\frac{\pi}{h}} \hat{U}(h\kappa) e^{ix_j\kappa} d\kappa \quad (\theta = h\kappa). \tag{2.7}$$

The transforms (2.6) and (2.7) are also known as *discrete-time Fourier Transform pair*. Starting from (2.4), with some manipulation, and using the transform definition in (2.6), we get, with $\lambda = \frac{k}{h}$ and $d = \frac{k}{h^2}$,

$$\hat{v}^{(l)}(\theta) \;=\; \frac{1}{1 + i\frac{a\lambda}{2}\sin\theta + 2d\sin^2\frac{\theta}{2}}\hat{v}^{(l-1)}(\theta).$$

Working similarly with (2.5), we get

$$\hat{v}^{(l)}(\theta) = \frac{1 - i\frac{a\lambda}{2}\sin\theta - 2d\sin^2\frac{\theta}{2}}{1 + i\frac{a\lambda}{2}\sin\theta + 2d\sin^2\frac{\theta}{2}}\hat{v}^{(l-1)}(\theta).$$

After $2R$ applications of (2.4) with time step-size $\frac{k}{2}$ followed by $m - R > 0$ applications of (2.5) with time step-size k, we have at terminal time $l = m$ (where $t_m = 1$),

$$\hat{v}^{(m)}(\theta) = z_1^m(\theta) z_2^R(\theta)\hat{v}^{(0)}(\theta), \tag{2.8}$$

with

$$z_1(\theta) = (1 - i\frac{a\lambda}{2}\sin\theta - 2d\sin^2\frac{\theta}{2})(1 + i\frac{a\lambda}{2}\sin\theta + 2d\sin^2\frac{\theta}{2})^{-1} \tag{2.9}$$

$$z_2(\theta) = (1 - i\frac{a\lambda}{2}\sin\theta - 2d\sin^2\frac{\theta}{2})^{-1}(1 + i\frac{a\lambda}{2}\sin\theta + 2d\sin^2\frac{\theta}{2})^{-1}. \tag{2.10}$$

3 Error Analysis of CN-Rannacher method

3.1 Review of Giles-Carter analysis [1]

Our analysis relies heavily on utilizing the sharp error estimates developed in [1] for linear PDEs with Dirac-delta initial data. In this section, we summarize the relevant results in [1]. We denote

$$\hat{U}^{(m)}(\theta) = z_1^m(\theta) z_2^R(\theta).$$

One can easily see $\hat{U}^{(m)}$ as the numerical timestepping operator up to time $t = 1$ in Fourier space given any initial $\hat{v}^{(0)}$. Algebraically, we write (here and in the rest of the paper) $\theta = h\kappa$.

The domain of κ is $[-\frac{\pi}{h}, \frac{\pi}{h}]$. Choose b such that $0 < b < \frac{1}{3}$ and c such that $\frac{1}{2} < c < 1$. For each h, we divide this domain of κ into three parts:

- Low frequency domain: $|\kappa| < h^{-b}$
- High frequency domain: $|\kappa| > h^{-c}$, and
- Mid frequency domain: $h^{-b} \le |\kappa| \le h^{-c}$.

Propositions 4.1, 4.2 and 4.3 in [1] show that the value of $\hat{U}^{(m)}(\theta)$ is more prominent in the low frequency domain than in the other two. In the low frequency domain, the value of $\hat{U}^{(m)}$ is of order $O(1)$. In the high frequency domain, the value of $\hat{U}^{(m)}$ is of order $O(h^{2R})$ where R is the number of fully implicit timesteps initially applied. Finally, the value of $\hat{U}^{(m)}$ in the mid frequency domain goes to zero faster than any polynomial in h, as $h \to 0$.

More specifically, for the low frequency domain, it is shown that

$$\hat{U}^{(m)}(\theta) = \hat{U}^{(m)}(h\kappa) = e^{-ia\kappa-\kappa^2}\left(1 + h^2 p(\kappa, a, \lambda, R)\right) + \text{ higher order terms} \tag{3.1}$$

where $p(\kappa, a, \lambda, R)$ of a specific polynomial form given in [1].

Consider the continuous Fourier transform (in x) of an L^1 function $f(t, x)$[1]:

$$\tilde{f}(t, \Psi) = \int_{-\infty}^{\infty} f(t, x)e^{-i\Psi x}dx. \tag{3.2}$$

[1] We denote $\tilde{f}$ to be the continuous Fourier transform of f, and $\hat{f}$ to be the discrete-time Fourier transform from samples of f.

Its inverse transform is given by

$$f(t,x) = \frac{1}{2\pi} \int_{-\infty}^{\infty} \tilde{f}(t,\Psi) e^{i\Psi x} d\Psi. \tag{3.3}$$

The analysis in [1] shows that the finite difference solution for (2.3) with Dirac-delta initial data has three components. The low-frequency component is of order $O(1)$ and differs from the true frequency representation by h^2. More specifically, for Dirac-delta $\delta(x)$ initial data (at $t = 0$), with $\delta(x) = 0$ if $x \neq 0$, and $\int_{\mathbb{R}} \delta(x)dx = 1$, we have $\tilde{v}(0,\Psi) = \tilde{\delta}(\Psi) = 1$ and so $\tilde{v}(1,\Psi) = e^{-ia\Psi-\Psi^2}$. This is to be compared with the low frequency region approximate (3.1). Substituting formally Ψ with κ, we see that the true frequency representation $\tilde{v}(1,\cdot)$ of $v(1,\cdot)$ is, therefore, of $O(h^2)$ difference with the representation $\hat{U}^{(m)}$ in (3.1).

Finally, when $R = 2$, the high frequency component in Proposition 4.2 in [1] is of order h^4, which can be shown to contribute to an $O(h^3)$ value in the spatial domain after performing an inverse transform. We assume $R = 2$ for the rest of our paper, and focus on the low frequency domain error.

In the following sections, we will study three types of non-smoothness of financial interest. We first illustrate our analysis for the solution of (2.3) with Dirac-delta initial condition, which is the continuous analogue of the price of an *Arrow-Debreu* security, also known as the state-price security, in financial theory. Next, we will consider the case when the initial condition is the Heaviside function, which is discontinuous at zero, corresponding to the payoff of a digital option. We will demonstrate how the discontinuity gives rise to a first order error that will dominate the second order error expected of a CN-Rannacher central difference method. Finally, we demonstrate the effect of the relative position of the point of non-smoothness on the leading error when the ramp function is the initial condition, even though it is continuous. In option pricing terminology, this initial condition is the payoff of a call option.

3.2 Dirac-delta function

We start with the analysis of the numerical solution of (2.3) with Dirac-delta initial condition. The Dirac-delta function $\delta(x)$ is a generalized function, defined formally by

- $\delta(x) = 0$ for $x \neq 0$
- $\int_{\mathbb{R}} \delta(x)dx = 1$.

Despite the singularity, the solution to (2.3) is smooth and is given by the Gaussian

$$v_\delta(t,x) = \frac{1}{\sqrt{4\pi t}} e^{-\frac{(x-at)^2}{4t}}. \tag{3.4}$$

Numerically, such an initial condition requires an approximation. Recall that our discretized grid is $x_j = (j + (1-\alpha))h$, where $j \in \{\ldots,-1,0,1,\ldots\} = \mathbf{Z}$. We shall use the following grid-dependent approximation of the Dirac-delta function:

$$v^{(0)}_{\delta,\alpha,h}(x_j) = \begin{cases} \frac{(1-\alpha)}{h} & \text{for } j = -1 \\ \frac{\alpha}{h} & \text{for } j = 0 \\ 0 & \text{else.} \end{cases} \tag{3.5}$$

The subscript δ in $v^{(0)}_{\delta,\alpha,h}$ indicates that it is an adaptation of the Dirac-delta function, while α and h indicate dependence on the discretized grid. The point of non-smoothness is at $x = 0$.

Equation (3.5) is by no means the only way to approximate the Dirac-delta function. A more detailed study on this point can be found in [14].

Applying the discrete-time Fourier transform (2.6) to (3.5), we obtain

$$\hat{v}^{(0)}_{\delta,\alpha,h}(\theta) = (1-\alpha)e^{i\alpha\theta} + \alpha e^{-i(1-\alpha)\theta}. \tag{3.6}$$

From (2.8) and Proposition 4.2 of [1], the value of $\hat{v}^{(m)}_{\delta,\alpha,h}(\theta) = \hat{v}^{(m)}_{\delta,\alpha,h}(h\kappa)$ in the high frequency component remains fourth order in h as $h \to 0$. This portion of the frequency domain then translates into an $O(h^3)$ value at any test point x^* in the spatial domain, since this high frequency domain contributes to the inverse Fourier transform by

$$\begin{aligned}
&\frac{1}{2\pi h}\Big|\int_{|\kappa|>h^{-c}} \hat{U}^{(m)}(\theta)\hat{v}^{(0)}_{\delta,\alpha,h}(\theta)e^{i\kappa x^*}d\kappa\Big| \\
\leq\ & \frac{1}{2\pi h}\Big|\int_{-\frac{\pi}{h}}^{\frac{\pi}{h}} \frac{(-1)^{m-2}h^4}{(2\lambda\sin^2\frac{\theta}{2})^4}e^{-\frac{1}{\lambda^2\sin^2(\frac{\theta}{2})}}(1+O(h\theta^{-2}))d\kappa\Big| \\
\leq\ & \frac{2h^3}{2\pi(2\lambda)^4}\int_0^{\pi}\frac{1}{\sin^8\frac{\theta}{2}}e^{-\frac{1}{\lambda^2\sin^2(\frac{\theta}{2})}}d\theta + \text{higher order terms} \quad (\theta=\kappa h) \\
=\ & O(h^3)
\end{aligned} \tag{3.7}$$

where the second last integral is finite by Appendix A in [1]. As a result, the dominating error term is $O(h^2)$ and is given by the low-frequency component. We rewrite (3.6) as

$$\begin{aligned}
\hat{v}^{(0)}_{\delta,\alpha,h}(\theta) &= (1-\alpha)e^{i\alpha\theta} + \alpha e^{-i(1-\alpha)\theta} \\
&= \tilde{v}^{(0)}_{\delta}(\kappa) - \frac{\alpha(1-\alpha)}{2}\kappa^2h^2 + O(h^3),
\end{aligned} \tag{3.8}$$

where $\tilde{v}^{(0)}_{\delta}(\kappa) \equiv \tilde{\delta}(\kappa) = 1$ is the continuous Fourier transform of the Dirac-delta function. As discussed, up to $O(h^2)$, we are only concerned with the low frequency component of $\hat{U}^{(m)}$, for $R = 2$. Therefore, using (2.7) and (3.1), an approximation of our finite difference solution $v^{(m)}_{\delta,\alpha,h}(x^*)$ at x^* is given by (modulo $O(h^3)$)[2]

$$\begin{aligned}
v^{(m)}_{\delta,\alpha,h}(x^*) &\approx \frac{1}{2\pi}\int_{-\frac{\pi}{h}}^{\frac{\pi}{h}} e^{-ia\kappa-\kappa^2}\Big(1+h^2p(\kappa,a,\lambda,R)\Big)\Big(\tilde{v}^{(0)}_{\delta}(\kappa) - \frac{\alpha(1-\alpha)}{2}\kappa^2h^2\Big)e^{i\kappa x^*}d\kappa \\
&\approx \frac{1}{2\pi}\int_{-\frac{\pi}{h}}^{\frac{\pi}{h}} e^{-ia\kappa-\kappa^2}e^{i\kappa x^*}\Big(\tilde{v}^{(0)}_{\delta}(\kappa) + h^2p(\kappa,a,\lambda,R)\tilde{v}^{(0)}_{\delta}(\kappa) - \frac{\alpha(1-\alpha)}{2}\kappa^2h^2\Big)d\kappa \\
&\approx \frac{1}{2\pi}\int_{-\infty}^{\infty} e^{-ia\kappa-\kappa^2}e^{i\kappa x^*}\Big(\tilde{v}^{(0)}_{\delta}(\kappa) + h^2p(\kappa,a,\lambda,R)\tilde{v}^{(0)}_{\delta}(\kappa) - \frac{\alpha(1-\alpha)}{2}\kappa^2h^2\Big)d\kappa \\
&\qquad\qquad \text{for } h \text{ small} \\
&= \frac{1}{2\pi}\int_{-\infty}^{\infty} e^{-ia\kappa-\kappa^2}e^{i\kappa x^*}\tilde{v}^{(0)}_{\delta}(\kappa)d\kappa + E^{(D)}_{\delta}(x^*) + E^{(Q)}_{\delta}(x^*) \\
&= v_\delta(1,x^*) + E^{(D)}_{\delta}(x^*) + E^{(Q)}_{\delta}(x^*),
\end{aligned} \tag{3.9}$$

[2] As $h \to 0$, the integral outside $[-\frac{\pi}{h}, \frac{\pi}{h}]$ is arbitrarily small and can be controlled by considering an asymptotic expansion of the error function $\mathrm{erfc}(x)$. Intuitively, this approximation from a finite integral to infinite integral holds as the Gaussian in the integrand $e^{-ia\kappa-\kappa^2}$ goes to zero faster than any polynomial as $h \to 0$.

Spatial step-size h	Time step-size k	FD Error	Error from (3.9)	Convergence rate estimate Υ (FD)
1/12	1/36	1.8962×10^{-4}	1.8932×10^{-4}	–
1/24	1/72	4.7349×10^{-5}	4.7329×10^{-5}	2.0017
1/48	1/144	1.1833×10^{-5}	1.1832×10^{-5}	2.0005
1/96	1/288	2.9581×10^{-6}	2.9581×10^{-6}	2.0001
1/192	1/576	7.3952×10^{-7}	7.3951×10^{-7}	2.0000

Table 3.1: Results of solving equation (2.3) with initial condition the Dirac-delta function $v^{(0)}_{\delta,\alpha,h}(x_j)$ (3.5). Solution evaluated at $x^* = 0.3$ with cubic spline interpolation. The speed of convection a is 0.5. Numerical method is CN-Rannacher timestepping with central spatial difference. Each grid is refined by inserting mid-points. Initially, the singularity is at a grid-point ($\alpha = 1$).

where v_δ is the exact solution to (2.3) with Dirac-delta initial data, and is given by (3.4). Therefore, the leading error of our finite difference solution at x^* is given by $E^{(D)}_\delta(x^*) + E^{(Q)}_\delta(x^*)$, where

$$E^{(D)}_\delta(x^*) \;=\; \frac{h^2}{2\pi}\int_{-\infty}^{\infty} e^{-ia\kappa-\kappa^2} e^{i\kappa x^*} p(\kappa, a, \lambda, R)\tilde{v}^{(0)}_\delta d\kappa \tag{3.10}$$

$$E^{(Q)}_\delta(x^*) \;=\; -\frac{h^2}{2\pi}\frac{\alpha(1-\alpha)}{2}\int_{-\infty}^{\infty} e^{-ia\kappa-\kappa^2} e^{i\kappa x^*}\kappa^2 d\kappa, \tag{3.11}$$

and the subscript δ indicates that this error is pertinent to Dirac-delta initial condition, approximated as in (3.5). It is helpful to think of $E^{(D)}_\delta$ as the inherent error from a CN-Rannacher discretization of the continuous problem. This error is present in the low frequency component and is invariant with respect to the positioning of the point of singularity.

The error $E^{(Q)}_\delta$ is in a similar spirit of the "quantization error" loosely defined in [11] as the error resulting from the resolution of the point of non-smoothness. This error, considered as a function of α, is a quadratic function that varies as the positioning of the singularity changes. For Dirac-delta initial condition, both these two errors can be explicitly calculated by elementary integration.

To illustrate this result, we take $\alpha = 1$ and compare our finite difference (FD) results with (3.9). Results are shown in Table 3.1. Here and in subsequent tables, "FD Error" will mean the error of our finite difference approximation compared to the known exact solution of the PDE. In Table 3.1, we notice a remarkable agreement between the "FD Error" and the error from our analysis as shown in (3.9).

As α is always 1 in Table 3.1, it turns out that the quantization error $E^{(Q)}$ is zero in all runs. What remains is the error term $E^{(D)}$, which is of second order. This is the optimal convergence order of CN-Rannacher with central differencing, and is experimentally observed in Table 3.1.

More interestingly, we start with $\alpha > 0$, and refine the grid by inserting mid-points so that the step-sizes are halved. Results in Table 3.2 show an unstable experimental convergence. Clearly, the error does not depend only on the spatial step-size, but also on the relative position of the singularity in the grid. While the error itself is *always* $O(h^2)$, the *coefficient* of the leading error term changes from one run to the next. With this particular way of refining the grid, the second order error is not experimentally observed.

This oscillatory behavior of convergence can be understood by looking at $E^{(Q)}_\delta$, which depends quadratically on α. The usual scheme of refining the grid by inserting mid-points will result in a dif-

Spatial step-size h	Time step-size k	FD Error	Error from (3.9)	Convergence rate estimate Υ (FD)
1/12	1/36	8.9209×10^{-5}	8.9528×10^{-5}	–
1/24	1/72	1.8841×10^{-5}	1.8818×10^{-5}	2.2433
1/48	1/144	7.0749×10^{-6}	7.0804×10^{-6}	1.4131
1/96	1/288	1.1758×10^{-6}	1.1761×10^{-6}	2.5891
1/192	1/576	4.4262×10^{-7}	4.4253×10^{-7}	1.4094

Table 3.2: Results of solving equation (2.3) with initial condition the Dirac-delta function $v^{(0)}_{\delta,\alpha,h}(x_j)$ (3.5). Solution evaluated at $x^* = 0.3$ with cubic spline interpolation. The speed of convection a is 0.5. Numerical method is CN-Rannacher timestepping with central spatial difference. Each grid is refined by inserting mid-points. Initially, the singularity is placed at a non grid-point ($\alpha = 0.7$).

ferent α from one run to the next. More precisely, from the $(l-1)$-th run to the (l)-th, we have

$$\alpha_l = \begin{cases} 2\alpha_{l-1} - 1 & \text{if } \alpha_{l-1} > 0.5 \\ 2\alpha_{l-1} & \text{if } \alpha_{l-1} \leq 0.5. \end{cases}$$

With α changing from one run to another, $E^{(Q)}_{\delta}$ does not exhibit a stable $O(h^2)$ convergence.

To summarize, for Dirac-delta initial condition, the approximation error depends not only on the step-sizes but also on the relative position of the singularity in the grid. We shall see that this dependence occurs for other examples we shall consider in this paper.

3.3 Heaviside function

The Heaviside function[3] is defined as

$$v^{(0)}_H(x) = \begin{cases} 1 & \text{if } x \geq 0 \\ 0 & \text{else.} \end{cases} \tag{3.12}$$

One would run into trouble when applying (2.6) directly to (3.12). This is because the series

$$\hat{v}_{H,\alpha,h}(\theta) = h \sum_{j=0}^{\infty} e^{-i(j+(1-\alpha))\theta} \tag{3.13}$$

does not converge for any $\theta \in \mathbb{R}$. Therefore, without a Fourier transform as in (2.6), it would be difficult to apply the theory in [1].

Fortunately, the fix is easy. Consider instead a *complex* θ. If the imaginary part of θ, is negative (i.e. $\mathrm{Im}(\theta) < 0$), then the geometric series (3.13) will converge as $|e^{-i\theta}| < 1$.

The transforms in (2.6), (2.7), (3.2) and (3.3) extend to complex-valued θ and correspondingly to $\kappa = \frac{\theta}{h}$ by considering contour integrals on horizontal lines in the complex plane. For real numbers ζ, define

$$C_\zeta = \{x + i\zeta, x \in [-\pi, \pi]\},$$

$$D_\zeta = \{x + i\zeta, x \in \mathbb{R}\}.$$

[3] In Section 2.1, the Heaviside function is denoted by $\mathcal{H}(\cdot)$, but, in this subsection and in what follows, we use $v^{(0)}_H(\cdot)$ for consistency with other subsections.

The only difference between C_ζ and D_ζ is that the former is a finite domain while the latter is infinite. Explicitly, for $\theta \in C_\zeta$, the discrete-time Fourier transform that takes a discrete sample of a function into a continuous spectrum of frequencies is

$$\hat{U}(\theta) = h \sum_{j=-\infty}^{\infty} U_j e^{-\frac{ix_j\theta}{h}}. \tag{3.14}$$

Its inverse transform is given by

$$U_j = \frac{1}{2\pi h} \int_{C_\zeta} \hat{U}(\theta) e^{\frac{ix_j\theta}{h}} d\theta. \tag{3.15}$$

Similarly, the continuous Fourier transform for $\Psi \in D_\zeta$ is

$$\tilde{f}(t,\Psi) = \int_{-\infty}^{\infty} f(t,x) e^{-i\Psi x} dx. \tag{3.16}$$

The inverse transform is given by

$$f(t,x) = \frac{1}{2\pi} \int_{D_\zeta} \tilde{f}(t,\Psi) e^{i\Psi x} d\Psi. \tag{3.17}$$

While the algebraic operations in Section 2.3 and in [1] mostly apply to the case of complex θ and κ, there are a few more key differences.
Firstly, we know that for $\theta \in \mathbb{R}$, the Crank-Nicolson timestepper z_1 satisfies

$$|z_1(\theta)| = |(1 - i\frac{a\lambda}{2}\sin\theta - 2d\sin^2\frac{\theta}{2})(1 + i\frac{a\lambda}{2}\sin\theta + 2d\sin^2\frac{\theta}{2})^{-1}| \leq 1.$$

This is no longer true for complex θ. We have, however, the following bound. Recall $\kappa = \frac{\theta}{h}$.

Proposition 3.1. *(Stability) Let $\theta \in C_{h\zeta}$ (in other words, $\zeta = \mathrm{Im}(\kappa)$ is fixed and independent of h). If the scaling $\frac{k}{h} = \lambda$ is maintained, then $|z_1(\theta)|^n$ is bounded independently of n and h.*

Proof. Write

$$\begin{aligned} \theta &= \mathrm{Re}(\theta) + i\,\mathrm{Im}(\theta) \\ \kappa &= \mathrm{Re}(\kappa) + i\,\mathrm{Im}(\kappa), \end{aligned}$$

where the two variables are again related by $\theta = h\kappa$. From (tedious) differentiation, the function $z_1(\theta)$, considered as a function of $\mathrm{Re}(\theta)$, attains its maximum at θ^* characterized by $\sin(\mathrm{Re}(\theta^*)) = 0$. As a result, the complex number $\sin(\theta^*)$ is purely imaginary. As $\zeta = \mathrm{Im}(\kappa)$ is assumed to be fixed, we have that $\sin(\theta^*) = \pm\frac{e^{-h\zeta}-e^{h\zeta}}{2i}$. For simplicity, take $\sin(\theta^*) = \frac{e^{-h\zeta}-e^{h\zeta}}{2i}$. Therefore,

$$\begin{aligned} |z_1(\theta)|^n &\leq |z_1(\theta^*)|^n \\ &= |(1 - \frac{1}{2}ia\lambda\sin\theta^* - 2d\sin^2\frac{\theta^*}{2})|^n|(1 + \frac{1}{2}ia\lambda\sin\theta^* + 2d\sin^2\frac{\theta^*}{2})|^{-n} \\ &= |1 - \frac{1}{2}a\lambda\frac{e^{-h\zeta}-e^{h\zeta}}{2} + 2d\frac{e^{-h\zeta}+e^{h\zeta}-2}{4}|^n \\ &\quad |1 + \frac{1}{2}a\lambda\frac{e^{-h\zeta}-e^{h\zeta}}{2} - 2d\frac{e^{-h\zeta}+e^{h\zeta}-2}{4}|^{-n} \\ &= |1 + \frac{1}{2}a\lambda h\zeta + \frac{\lambda}{h}\frac{h^2\zeta^2 + O(h^4)}{2}|^{\frac{1}{\lambda h}}|1 - \frac{1}{2}a\lambda h\zeta - \frac{\lambda}{h}\frac{h^2\zeta^2 + O(h^4)}{2}|^{\frac{1}{\lambda h}} \\ &\to \exp(a\zeta + \zeta^2), \end{aligned}$$

as $h \to 0$. ∎

The analysis in [1] goes through for complex θ and correspondingly $\kappa = \frac{\theta}{h}$, with the following modifications:

- The Taylor series for the logarithm could have an additional term which would be an integral multiple of $2\pi i$, due to the complex logarithm being a multi-valued function. This does not affect the argument as the subsequent exponentiation will yield the same result regardless ($e^{2\pi i} = 1$).
- Following the proof of Proposition 3.1, the maximum and the minimum points of $z_1(\theta)$ as a function of $\mathrm{Re}(\theta)$ can be similarly identified. The rest of the argument goes through.

We fix $\zeta = \mathrm{Im}(\kappa) < 0$ and consider $\theta = h\kappa$. As $\mathrm{Im}(\theta) < 0$,

$$\hat{v}^{(0)}_{H,\alpha,h}(\theta) = h\sum_{j=0}^{\infty} e^{-i(j+(1-\alpha))\theta} = \frac{he^{-i(1-\alpha)\theta}}{1-e^{-i\theta}}. \tag{3.18}$$

The continuous Fourier transform (3.2) of the Heaviside function is given by

$$\tilde{v}^{(0)}_H(\kappa) = \int_0^{\infty} e^{-i\kappa x}dx = \frac{1}{i\kappa}. \tag{3.19}$$

Substituting $\theta = h\kappa$ in (3.18), Taylor series expansion yields

$$\hat{v}^{(0)}_{H,\alpha,h}(h\kappa) = \tilde{v}^{(0)}_H(\kappa) + (\alpha - \frac{1}{2})h + \frac{i\kappa h^2}{2}(\alpha^2 - \alpha + \frac{1}{6}) + O(h^3).$$

It is not hard to prove that the high-frequency error is again $O(h^3)$ when two Rannacher timesteps are used ($R = 2$). As a result, up to $O(h^2)$, for h small, our finite difference solution is

$$\begin{aligned}
v^{(m)}_{H,\alpha,h}(x^*) &\approx \frac{1}{2\pi}\int_{D_\zeta} e^{-ia\kappa-\kappa^2}\Big(1 + h^2 p(\kappa, a, \lambda, R)\Big) \\
&\quad \times\Big(\tilde{v}^{(0)}_H(\kappa) + (\alpha - \frac{1}{2})h + \frac{i\kappa h^2}{2}(\alpha^2 - \alpha + \frac{1}{6})\Big)e^{i\kappa x^*}d\kappa \\
&\approx \frac{1}{2\pi}\int_{D_\zeta} e^{-ia\kappa-\kappa^2}e^{i\kappa x^*}\Big(\tilde{v}^{(0)}_H(\kappa) + h^2 p(\kappa, a, \lambda, R)\tilde{v}^{(0)}_H(\kappa) \\
&\quad +(\alpha - \frac{1}{2})h + \frac{i\kappa h^2}{2}(\alpha^2 - \alpha + \frac{1}{6})\Big)d\kappa \\
&= \frac{1}{2\pi}\int_{D_\zeta} e^{-ia\kappa-\kappa^2}e^{i\kappa x^*}\tilde{v}^{(0)}_H(\kappa)d\kappa + E^{(D)}_H(x^*) + E^{(Q)}_H(x^*) \\
&= v_H(1, x^*) + E^{(D)}_H(x^*) + E^{(Q)}_H(x^*),
\end{aligned} \tag{3.20}$$

where $E^{(D)}_H(x^*)$ and $E^{(Q)}_H(x^*)$ are analogously given by

$$E^{(D)}_H(x^*) = \frac{h^2}{2\pi}\int_{D_\zeta} e^{-ia\kappa-\kappa^2}e^{i\kappa x^*}p(\kappa, a, \lambda, R)\tilde{v}^{(0)}_H d\kappa \tag{3.21}$$

$$\begin{aligned}
E^{(Q)}_H(x^*) &= \frac{h}{2\pi}(\alpha - \frac{1}{2})\int_{D_\zeta} e^{-ia\kappa-\kappa^2}e^{i\kappa x^*}d\kappa \\
&\quad +\frac{ih^2}{4\pi}(\alpha^2 - \alpha + \frac{1}{6})\int_{D_\zeta} e^{-ia\kappa-\kappa^2}e^{i\kappa x^*}\kappa d\kappa.
\end{aligned} \tag{3.22}$$

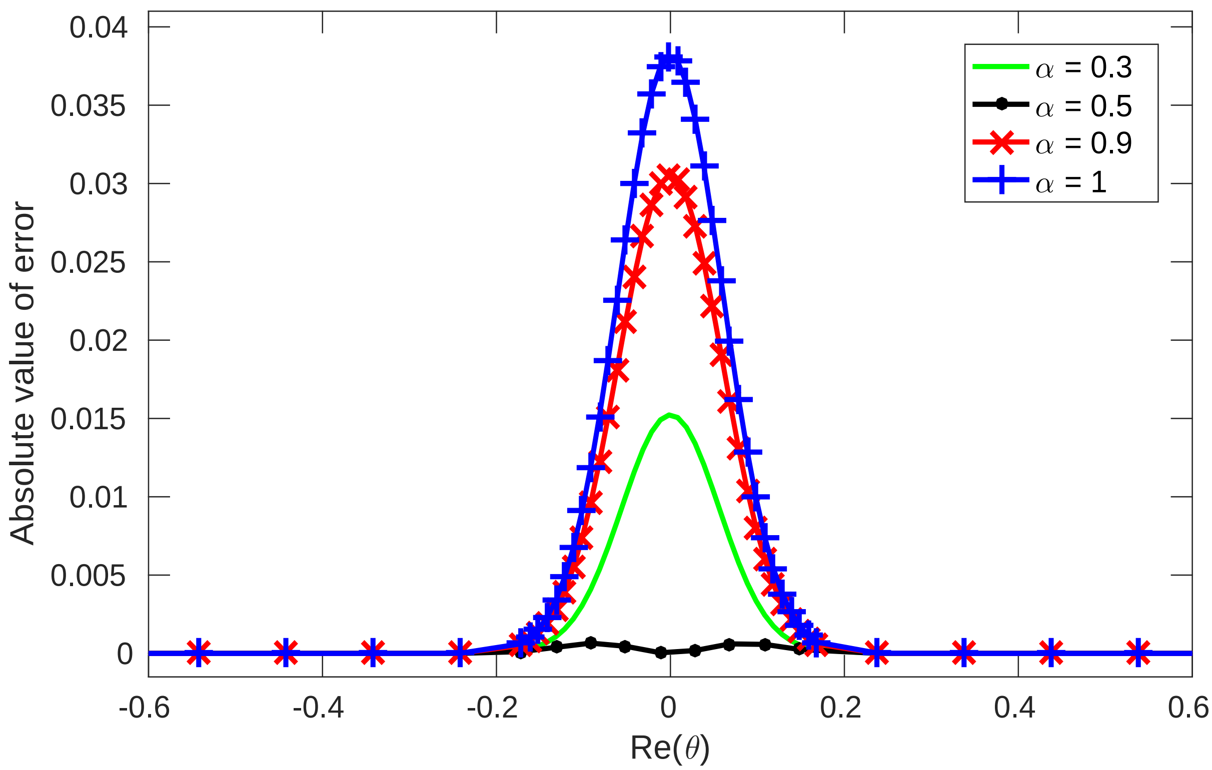

Figure 3.1: The error of our finite difference approximation in frequency space, at $t = 1$. Parameters: $a = 1, \lambda = \frac{1}{3}, h = \frac{1}{12}$. The imaginary part of κ is fixed to -0.1.

In other words, the quantization error[4] is first order in h. The relative position of the discontinuity on the grid has a more prominent effect than the "usual" timestepping error from CN-Rannacher timestepping, and cannot be damped by the initial backward Euler integrations. In the lower end of the frequency space, it corresponds to a shift by a Gaussian. Figure 3.1 shows this phenomenon.

Again, it is straightforward to obtain the integrals in $E_H^{(Q)}$ or $E_H^{(D)}$ exactly or numerically. In Table 3.3, we show the agreement between the numerical solution error and the error as approximated in (3.20). As expected, the convergence is only linear when the point of discontinuity is placed at a grid-point.

Considered as a function in α, the $O(h)$-term in the quantization error $E_H^{(Q)}$ is directly proportional to $(\alpha - \frac{1}{2})$, and vanishes when $\alpha = \frac{1}{2}$. A corollary is that, placing the discontinuity at grid-point is the worst possible choice in terms of minimizing error. The farther the discontinuity is away from the mid-point, the larger the first order error will be. This is illustrated in Table 3.4. In each refinement, we use a mesh that has the required α and spatial step-size h, and compute our finite difference solution based on such a grid. Table 3.4 shows that, with essentially the same computational effort, the grid placement has a direct and prominent effect on the efficiency of the numerical method.

This particular form of $E_H^{(Q)}$ also explains why the errors in Table 2.1 are larger than the errors in Table 2.2, despite the more stable convergence of the former. As $|\alpha - \frac{1}{2}|$ is maximized when $\alpha = 0$ or $\alpha = 1$, the error of our finite difference approximation is also maximized when the discontinuity is placed at a grid-point, other things equal.

[4]To be precise, $E_H^{(Q)}$ also contains the difference between the discrete and continuous Fourier transforms.

Spatial step-size h	Time step-size k	FD Error	Error from (3.20)	Convergence rate estimate Υ (FD)
1/12	1/24	1.0504×10^{-2}	1.0492×10^{-2}	–
1/24	1/48	5.2241×10^{-3}	5.2227×10^{-3}	1.0076
1/48	1/96	2.6057×10^{-3}	2.6055×10^{-3}	1.0035
1/96	1/192	1.3013×10^{-3}	1.3013×10^{-3}	1.0017
1/192	1/384	6.5029×10^{-4}	6.5029×10^{-4}	1.0008

Table 3.3: Results of solving equation (2.3) with initial condition the Heaviside function $v_H^{(0)}(x)$ (3.12). Solution evaluated at $x^* = 0$. The speed of convection a is 0.7. Numerical method is CN-Rannacher timestepping with central spatial difference. Each grid is refined by inserting mid-points. Initially, the discontinuity is at a grid-point ($\alpha = 1$).

Spatial step-size h	Time step-size k	$\alpha = 0.3$	$\alpha = 0.5$	$\alpha = 0.9$	$\alpha = 1$
1/12	1/24	-4.1349×10^{-3}	1.7457×10^{-5}	8.3946×10^{-3}	1.0504×10^{-2}
1/24	1/48	-2.0730×10^{-3}	4.3549×10^{-6}	4.1772×10^{-3}	5.2241×10^{-3}
1/48	1/96	-1.0381×10^{-3}	1.0882×10^{-6}	2.0840×10^{-3}	2.6057×10^{-3}
1/96	1/192	-5.1949×10^{-4}	2.7201×10^{-7}	1.0409×10^{-3}	1.3013×10^{-3}
1/192	1/384	-2.5986×10^{-4}	6.7999×10^{-8}	5.2020×10^{-4}	6.5029×10^{-4}
Approximated Convergence		Linear	Quadratic	Linear	Linear

Table 3.4: Results of solving equation (2.3) with initial condition the Heaviside function $v_H^{(0)}(x)$ (3.12). Solution evaluated at $x^* = 0$. The speed of convection a is 0.7. Numerical method is CN-Rannacher timestepping with central spatial difference. The relative position α is maintained at each run.

3.4 Call and put type initial conditions

We consider the following functions:

$$
\begin{aligned}
v_C^{(0)}(x) &= \max(x,0) \quad \text{(Call)} && (3.23)\\
v_P^{(0)}(x) &= \max(-x,0) \quad \text{(Put)} && (3.24)\\
v_{EC}^{(0)}(x) &= \max(e^x-1,0) \quad \text{(Exponential Call)} && (3.25)\\
v_{EP}^{(0)}(x) &= \max(1-e^x,0) \quad \text{(Exponential Put)} && (3.26)
\end{aligned}
$$

These functions are continuous but not continuously differentiable. The exponential call and put functions are related to solving for the value of a call/put option under geometric Brownian motion, after a log transform.

Similarly to Section 3.3, we can consider the complex extension of the Fourier transform, i.e. (3.14) to (3.17). In order for the series to converge, we require that

$$
\begin{aligned}
\mathrm{Im}(\theta) < 0 \;&\Leftrightarrow\; \mathrm{Im}(\kappa) < 0 \quad \text{for call} && (3.27)\\
\mathrm{Im}(\theta) < -h \;&\Leftrightarrow\; \mathrm{Im}(\kappa) < -1 \quad \text{for exponential call} && (3.28)\\
\mathrm{Im}(\theta) > 0 \;&\Leftrightarrow\; \mathrm{Im}(\kappa) > 0 \quad \text{for put/exponential put.} && (3.29)
\end{aligned}
$$

3.4.1 Call and put

For θ such that $\mathrm{Im}(\theta) < 0$, the discrete-time Fourier transform of the ramp function (3.23) is

$$\hat{v}_{C,\alpha,h}^{(0)}(\theta) = h^2 \sum_{j=0}^{\infty} (j+(1-\alpha))e^{-i(j+(1-\alpha))\theta} = h^2 e^{-i(1-\alpha)\theta}\left(\frac{1-\alpha}{1-e^{-i\theta}} + \frac{e^{-i\theta}}{(1-e^{-i\theta})^2}\right). \tag{3.30}$$

This is to be compared with the continuous Fourier transform of (3.23), which for $\mathrm{Im}(\kappa) < 0$ is given by

$$\tilde{v}_C^{(0)}(\kappa) = \int_0^\infty x e^{-i\kappa x} dx = -\frac{1}{\kappa^2}. \tag{3.31}$$

Substituting $\theta = h\kappa$ in (3.30), Taylor series expansion yields

$$\hat{v}_{C,\alpha,h}^{(0)}(h\kappa) = \tilde{v}_C^{(0)}(\kappa) + h^2\left(-\frac{\alpha^2}{2} + \frac{\alpha}{2} - \frac{1}{12}\right) + O(h^3). \tag{3.32}$$

Let $\zeta_1 < 0$. By repeating the argument in Section 3.3, we have the expression of our finite difference solution

$$
\begin{aligned}
v_{C,\alpha,h}^{(m)}(x^*) &\approx \frac{1}{2\pi}\int_{D_{\zeta_1}} e^{-ia\kappa-\kappa^2}\Big(1+h^2 p(\kappa,a,\lambda,R)\Big)\\
&\quad \times\left(\tilde{v}_C^{(0)}(\kappa) + h^2\left(-\frac{\alpha^2}{2}+\frac{\alpha}{2}-\frac{1}{12}\right)\right)e^{i\kappa x^*}d\kappa\\
&= \frac{1}{2\pi}\int_{D_{\zeta_1}} e^{-ia\kappa-\kappa^2}e^{i\kappa x^*}\tilde{v}_C^{(0)}(\kappa)d\kappa + E_C^{(D)}(x^*) + E_C^{(Q)}(x^*)\\
&= v_C(1,x^*) + E_C^{(D)}(x^*) + E_C^{(Q)}(x^*), && (3.33)
\end{aligned}
$$

where $E_C^{(D)}(x^*)$ and $E_C^{(Q)}(x^*)$ are given by

$$E_C^{(D)}(x^*) = \frac{h^2}{2\pi}\int_{D_{\zeta_1}} e^{-ia\kappa-\kappa^2}e^{i\kappa x^*}p(\kappa,a,\lambda,R)\tilde{v}_C^{(0)}d\kappa \quad (3.34)$$

$$E_C^{(Q)}(x^*) = \frac{h^2}{2\pi}(-\frac{\alpha^2}{2}+\frac{\alpha}{2}-\frac{1}{12})\int_{D_{\zeta_1}} e^{-ia\kappa-\kappa^2}e^{i\kappa x^*}d\kappa. \quad (3.35)$$

As a result, even though a second order error is to be expected from a CN-Rannacher discretization, the coefficient of the error depends (quadratically) on the placement of the point of non-smoothness in the grid. In both the frequency space and the original mesh, this error corresponds to a shift by a Gaussian.

Incidentally, for $R=2$, the spatial error due to high frequency component for the call is not $O(h^3)$, but in fact $O(h^5)$. This is because

$$\tilde{v}_C^{(0)}(\kappa) = -\frac{1}{\kappa^2} = -\frac{h^2}{\theta^2},$$

which adds two orders in h to the high frequency component, in a calculation similar to (3.7):

$$\begin{aligned}
&\frac{1}{2\pi h}\left|\int_{|\kappa|>h^{-c}} \hat{U}^{(m)}(\theta)\hat{v}_{\delta,\alpha,h}(\theta)e^{i\kappa x^*}d\kappa\right| \\
\leq\ & \frac{1}{2\pi h}\left|\int_{-\frac{\pi}{h}}^{\frac{\pi}{h}} \frac{(-1)^{m-2}h^6}{(2\lambda\sin^2\frac{\theta}{2})^4\theta^2}e^{-\frac{1}{\lambda^2\sin^2(\frac{\theta}{2})}}(1+O(h\theta^{-2}))d\kappa\right| \quad (3.36)\\
\leq\ & \frac{1}{(2\lambda)^4\pi}\int_0^{\pi}\frac{h^5}{\theta^2\sin^8\frac{\theta}{2}}e^{-\frac{1}{\lambda^2\sin^2(\frac{\theta}{2})}}d\theta + \text{higher order terms} \quad (\theta=\kappa h)\\
=\ & O(h^5).
\end{aligned}$$

Coming to the put initial conditions, we compute the discrete-time and continuous Fourier transforms of (3.24) for $\mathrm{Im}(\theta)>0$ and $\mathrm{Im}(\kappa)>0$. It turns out that

$$\hat{v}_{P,\alpha,h}^{(0)}(\theta) = h^2\sum_{j=-\infty}^{-1}(-(j+(1-\alpha)))e^{-i(j+(1-\alpha))\theta)} = h^2e^{-i(1-\alpha)\theta}\left(\frac{-(1-\alpha)e^{i\theta}}{1-e^{i\theta}}+\frac{e^{i\theta}}{(1-e^{i\theta})^2}\right), \quad (3.37)$$

and

$$\tilde{v}_P^{(0)}(\kappa) = -\int_{-\infty}^{0} xe^{-i\kappa x}dx = -\frac{1}{\kappa^2}. \quad (3.38)$$

Substituting $\theta = h\kappa$ in (3.37), Taylor series expansion yields

$$\hat{v}_{P,\alpha,h}^{(0)}(h\kappa) = \tilde{v}_P^{(0)}(\kappa) + h^2(-\frac{\alpha^2}{2}+\frac{\alpha}{2}-\frac{1}{12}) + O(h^3). \quad (3.39)$$

Interestingly, the initial conditions (3.32) and (3.39) have the same transform, even though they are *defined* on different regions on the complex plane.
Let $\zeta_2>0$. Our finite difference solution under CN-Rannacher timestepping is

$$\begin{aligned}
v_{P,\alpha,h}^{(m)}(x^*) &\approx \frac{1}{2\pi}\int_{D_{\zeta_2}} e^{-ia\kappa-\kappa^2}\left(1+h^2p(\kappa,a,\lambda,R)\right)\\
&\quad\times\left(\tilde{v}_P^{(0)}(\kappa)+h^2(-\frac{\alpha^2}{2}+\frac{\alpha}{2}-\frac{1}{12})\right)e^{i\kappa x^*}d\kappa\\
&= \frac{1}{2\pi}\int_{D_{\zeta_2}} e^{-ia\kappa-\kappa^2}e^{i\kappa x^*}\tilde{v}_P^{(0)}(\kappa)d\kappa + E_P^{(D)}(x^*) + E_P^{(Q)}(x^*)\\
&= v_P(1,x^*) + E_P^{(D)}(x^*) + E_P^{(Q)}(x^*), \quad (3.40)
\end{aligned}$$

where $E_P^{(D)}(x^*)$ and $E_P^{(Q)}(x^*)$ are given by

$$E_P^{(D)}(x^*) = \frac{h^2}{2\pi}\int_{D_{\zeta_2}} e^{-ia\kappa-\kappa^2}e^{i\kappa x^*}p(\kappa,a,\lambda,R)\tilde{v}_P^{(0)}d\kappa \tag{3.41}$$

$$E_P^{(Q)}(x^*) = \frac{h^2}{2\pi}(-\frac{\alpha^2}{2}+\frac{\alpha}{2}-\frac{1}{12})\int_{D_{\zeta_2}} e^{-ia\kappa-\kappa^2}e^{i\kappa x^*}d\kappa. \tag{3.42}$$

We also have that

$$p(\kappa,a,\lambda,R)\times(-\frac{1}{\kappa^2}) = -\frac{1}{6}ia\kappa - \frac{1}{12}\kappa^2 + \frac{1}{12}\lambda^2\kappa(ia+\kappa)^3 - \frac{1}{4}R\lambda^2(ia+\kappa)^2$$

is analytic as a function of κ. As a result,

$$E_C^{(D)}(x^*) = E_P^{(D)}(x^*), \quad \text{and}$$
$$E_C^{(Q)}(x^*) = E_P^{(Q)}(x^*).$$

In other words, at least up to second order, the error of CN-Rannacher is the same for the call and the put. This is to be expected, as it is easy to prove that

$$v_C(t,x) - v_P(t,x) = x - at,$$

and that our numerical scheme is exact on linear functions. This numerical phenomenon does not occur for the exponential call and put, as we shall see in the next section.

3.4.2 Exponential call and put

Consider now the exponential call as the initial condition to (2.3), given by (3.25). Its discrete-time Fourier transform for $\mathrm{Im}(\theta) < -h$ is

$$\hat{v}_{EC,\alpha,h}^{(0)}(\theta) = h\sum_{j=0}^{\infty}(e^{(j+(1-\alpha))h}-1)e^{-i(j+(1-\alpha))\theta)} = he^{-i(1-\alpha)\theta}\left(\frac{e^{(1-\alpha)h}}{1-e^{-i\theta+h}} - \frac{1}{1-e^{-i\theta}}\right). \tag{3.43}$$

Its continuous Fourier transform is, for $\mathrm{Im}(\kappa) < -1$,

$$\tilde{v}_{EC}^{(0)}(\kappa) = \int_0^{\infty}(e^x-1)e^{-i\kappa x}dx = \frac{1}{i\kappa(i\kappa-1)}. \tag{3.44}$$

Substituting $\theta = h\kappa$ in (3.43), Taylor series expansion yields

$$\hat{v}_{EC,\alpha,h}^{(0)}(h\kappa) = \tilde{v}_{EC}^{(0)}(\kappa) + h^2(-\frac{\alpha^2}{2}+\frac{\alpha}{2}-\frac{1}{12}) + O(h^3). \tag{3.45}$$

Comparing (3.45) with (3.32), we see that the quantization error (the E_Q-component) of an exponential call is the same as the one for the corresponding (non-exponential) call.

Let $\zeta_1 < -1$. By repeating the argument in Section 3.4.1, we have the following expression of our finite difference solution

$$\begin{aligned} v_{EC,\alpha,h}^{(m)}(x^*) &\approx \frac{1}{2\pi}\int_{D_{\zeta_1}} e^{-ia\kappa-\kappa^2}\left(1+h^2p(\kappa,a,\lambda,R)\right) \\ &\quad \times\left(\tilde{v}_{EC}^{(0)}(\kappa) + h^2(-\frac{\alpha^2}{2}+\frac{\alpha}{2}-\frac{1}{12})\right)e^{i\kappa x^*}d\kappa \\ &= \frac{1}{2\pi}\int_{D_{\zeta_1}} e^{-ia\kappa-\kappa^2}e^{i\kappa x^*}\tilde{v}_{EC}^{(0)}(\kappa)d\kappa + E_{EC}^{(D)}(x^*) + E_{EC}^{(Q)}(x^*) \\ &= v_{EC}(1,x^*) + E_{EC}^{(D)}(x^*) + E_{EC}^{(Q)}(x^*), \end{aligned} \tag{3.46}$$

where $E^{(D)}_{EC}(x^*)$ and $E^{(Q)}_{EC}(x^*)$ are given by

$$E^{(D)}_{EC}(x^*) = \frac{h^2}{2\pi}\int_{D_{\zeta_1}} e^{-ia\kappa-\kappa^2}e^{i\kappa x^*}p(\kappa,a,\lambda,R)\tilde{v}^{(0)}_{EC}d\kappa \quad (3.47)$$

$$E^{(Q)}_{EC}(x^*) = \frac{h^2}{2\pi}(-\frac{\alpha^2}{2}+\frac{\alpha}{2}-\frac{1}{12})\int_{D_{\zeta_1}} e^{-ia\kappa-\kappa^2}e^{i\kappa x^*}d\kappa. \quad (3.48)$$

Similarly, for $\mathrm{Im}(\theta) > 0$ and $\mathrm{Im}(\kappa) > 0$, the discrete-time and continuous transforms for the exponential put are

$$\hat{v}^{(0)}_{EP,\alpha,h}(\theta) = h\sum_{j=-\infty}^{-1}(1-e^{(j+(1-\alpha))h})e^{-i(j+(1-\alpha))\theta)} = he^{-i(1-\alpha)\theta}\left(\frac{e^{i\theta}}{1-e^{i\theta}}-\frac{e^{(1-\alpha)h+i\theta-h}}{1-e^{i\theta-h}}\right), \quad (3.49)$$

and

$$\tilde{v}^{(0)}_{EP}(\kappa) = \int_{-\infty}^{0}(1-e^{x})e^{-i\kappa x}dx = \frac{1}{i\kappa(i\kappa-1)}. \quad (3.50)$$

Substituting $\theta = h\kappa$ into (3.49), once again Taylor series expansion yields

$$\hat{v}^{(0)}_{EP,\alpha,h}(h\kappa) = \tilde{v}^{(0)}_{EP}(\kappa) + h^2(-\frac{\alpha^2}{2}+\frac{\alpha}{2}-\frac{1}{12}) + O(h^3). \quad (3.51)$$

For $\zeta_2 > 0$, we have the following expression of our finite difference solution for the exponential put

$$\begin{aligned} v^{(m)}_{EP,\alpha,h}(x^*) &\approx \frac{1}{2\pi}\int_{D_{\zeta_2}} e^{-ia\kappa-\kappa^2}\Big(1+h^2p(\kappa,a,\lambda,R)\Big) \\ &\quad\times\Big(\tilde{v}^{(0)}_{EP}(\kappa)+h^2(-\frac{\alpha^2}{2}+\frac{\alpha}{2}-\frac{1}{12})\Big)e^{i\kappa x^*}d\kappa \\ &= \frac{1}{2\pi}\int_{D_{\zeta_2}} e^{-ia\kappa-\kappa^2}e^{i\kappa x^*}\tilde{v}^{(0)}_{EP}(\kappa)d\kappa + E^{(D)}_{EP}(x^*) + E^{(Q)}_{EP}(x^*) \\ &= v_{EP}(1,x^*) + E^{(D)}_{EP}(x^*) + E^{(Q)}_{EP}(x^*), \end{aligned} \quad (3.52)$$

where $E^{(D)}_{EP}(x^*)$ and $E^{(Q)}_{EP}(x^*)$ are given by

$$E^{(D)}_{EP}(x^*) = \frac{h^2}{2\pi}\int_{D_{\zeta_2}} e^{-ia\kappa-\kappa^2}e^{i\kappa x^*}p(\kappa,a,\lambda,R)\tilde{v}^{(0)}_{EP}d\kappa \quad (3.53)$$

$$E^{(Q)}_{EP}(x^*) = \frac{h^2}{2\pi}(-\frac{\alpha^2}{2}+\frac{\alpha}{2}-\frac{1}{12})\int_{D_{\zeta_2}} e^{-ia\kappa-\kappa^2}e^{i\kappa x^*}d\kappa. \quad (3.54)$$

Obviously, as their corresponding integrands are analytic, we have

$$E^{(Q)}_{EC}(x^*) = E^{(Q)}_{EP}(x^*),$$

in other words, the leading quantization errors are equal. However, because of a pole at $\kappa = -i$, it holds that $E^{(D)}_{EC}(x^*) \neq E^{(D)}_{EP}(x^*)$. To see this, consider a positively oriented contour Γ consisting of the following segments, for some $M > 0$:

$$\begin{aligned} \Gamma_1 &= \{x+i\zeta_1 | -M \le x \le M\} \\ \Gamma_2 &= \{M+iy| \ \ \zeta_1 \le y \le \zeta_2\} \\ \Gamma_3 &= \{x+i\zeta_2 | -M \le x \le M\} \\ \Gamma_4 &= \{-M+iy| \ \zeta_1 \le y \le \zeta_2\}. \end{aligned}$$

Spatial step-size h	Time step-size k	FD Error	Error from (3.55)	Convergence rate estimate Υ (FD)
1/12	1/24	-2.0221×10^{-4}	-2.0174×10^{-4}	–
1/24	1/48	-5.0466×10^{-5}	-5.0434×10^{-5}	2.0025
1/48	1/96	-1.2610×10^{-5}	-1.2609×10^{-5}	2.0007
1/96	1/192	-3.1523×10^{-6}	-3.1521×10^{-6}	2.0001
1/192	1/384	-7.8804×10^{-7}	-7.8803×10^{-7}	2.0001

Table 3.5: Results of solving equation (2.3) with initial condition the exponential forward $v_F^{(0)}(x)$ (3.56). Solution evaluated at $x^* = 0$. The speed of convection a is 0.7. Numerical method is CN-Rannacher timestepping with central spatial difference. Each grid is refined by inserting mid-points. Initially, we set $\alpha = 0.7$.

By Cauchy's residue theorem, we have

$$\int_\Gamma e^{-iaz-z^2} e^{izx^*} \frac{p(z,a,\lambda,R)}{iz(iz-1)} dz \quad = \quad -2\pi i \left[e^{-iaz-z^2} e^{izx^*} \frac{p(z,a,\lambda,R)}{z} \right]_{z=-i}.$$

The last quantity is readily computable as $\frac{p(z,a,\lambda,R)}{z}$ itself is a polynomial in z. Finally, as $M \to \infty$, we note that the contributions from Γ_2 and Γ_4 vanish and

$$\int_{\Gamma_1} e^{-ia\kappa-\kappa^2} e^{i\kappa x^*} p(\kappa,a,\lambda,R) \tilde{v}_{EC}^{(0)} d\kappa \to \int_{D_{\zeta_1}} e^{-ia\kappa-\kappa^2} e^{i\kappa x^*} p(\kappa,a,\lambda,R) \tilde{v}_{EC}^{(0)} d\kappa$$

and similarly

$$-\int_{\Gamma_3} e^{-ia\kappa-\kappa^2} e^{i\kappa x^*} p(\kappa,a,\lambda,R) \tilde{v}_{EP}^{(0)} d\kappa \to -\int_{D_{\zeta_2}} e^{-ia\kappa-\kappa^2} e^{i\kappa x^*} p(\kappa,a,\lambda,R) \tilde{v}_{EP}^{(0)} d\kappa$$

Therefore, we have

$$\begin{aligned} E_{EC}^{(D)}(x^*) - E_{EP}^{(D)}(x^*) &= -h^2 i \left[e^{-iaz-z^2} e^{izx^*} \frac{p(z,a,\lambda,R)}{z} \right]_{z=-i} \\ &= -h^2 e^{x-a+1} \left(\frac{a}{6} - \frac{1}{12} + \frac{1}{12}\lambda^2 (a-1)^3 - \frac{1}{4} R \lambda^2 (a-1)^2 \right). \end{aligned} \tag{3.55}$$

As $E_{EC}^{(Q)}(x^*) = E_{EP}^{(Q)}(x^*)$, the quantity $E_{EC}^{(D)}(x^*) - E_{EP}^{(D)}(x^*)$ is in fact the second order error of solving (2.3) with the initial condition

$$v_F^{(0)}(x) = e^x - 1 \tag{3.56}$$

under CN-Rannacher timestepping[5]. In financial context, this initial condition is the payoff of a forward contract under the geometric Brownian motion model. As the quantization error is cancelled out, the relative position of the strike on the grid is no longer relevant in the second order error, and the leading error depends (computationally) only on the time and spatial step size. This is illustrated in Table 3.5.

[5] This connection between the values of put, call and forward via integration across complex poles is a form of put-call parity [6].

Spatial step-size h	Time step-size k	FD Error	Convergence rate estimate Υ (FD)
1/12	1/24	9.3332×10^{-7}	–
1/24	1/48	1.1988×10^{-7}	2.9608
1/48	1/96	1.5140×10^{-8}	2.9851
1/96	1/192	1.8924×10^{-9}	3.0001
1/192	1/384	2.3323×10^{-10}	3.0205

Table 4.1: Results of solving equation (2.3) with initial condition the exponential put $v_{EP}^{(0)}(x)$ (3.26). Solution evaluated at $x^* = 0$ with cubic spline interpolation. The speed of convection a is -0.3. Numerical method is CN-Rannacher timestepping with central spatial difference. The relative position of the strike is maintained at $\alpha = 0.37853$.

Initial condition	Optimal α to eliminate the leading term of $E^{(Q)}$	Point of the extremum of the quadratic $E^{(D)} + E^{(Q)}$
Dirac-delta	0 or 1	0.5
Heaviside	0.5	not applicable (linear)
Usual Call, Put and Exponential Call, Put	$\frac{1}{2} - \sqrt{\frac{1}{12}} \approx 0.2113$ or $\frac{1}{2} + \sqrt{\frac{1}{12}} \approx 0.7887$	0.5

Table 4.2: Special choices of α.

4 On choosing α

The analysis from Sections 3.2 to 3.4 suggests that as long as the relative position of the point of non-smoothness on the grid is maintained, the convergence order is stable. The next question is to determine an optimal α such that the error is minimized.

This is complicated by the fact that, while α directly influences $E^{(Q)}$, the other term in the error $E^{(D)}$ is independent of α. It is possible to use the quantization error $E^{(Q)}$ to our advantage. For the initial conditions considered in this paper, one could consider the error $E^{(D)} + E^{(Q)}$ as a quadratic function in α. In some cases, the leading error term could be completely eliminated by a good choice of α, leading to *super-convergence* by a second order finite difference scheme (see Table 4.1).

This technique of choosing α to obtain a superconvergence does not seem to be possible in practical situations, as a detailed study of $E^{(D)}$ and $E^{(Q)}$ seems necessary to determine the α for which superconvergence occurs. In addition, such an α that cancels the leading second order term may not exist. Instead, we proceed to minimize merely $E^{(Q)}$. Consider $E^{(Q)}$ as a function in α in itself, one can minimize its absolute value and obtain the estimates as listed in Table 4.2. For the case of call and put, often the combined error $E^{(D)} + E^{(Q)}$ has no root, considered as a function of α. In those cases, the mid-point minimizes the overall error. We remark that these numbers seem to confirm the empirical findings of [7], in which the authors found experimentally that the optimal value of α lies in $(0.2, 0.3)$ or $(0.7, 0.8)$ for the call option, and 0.5 for the bet option (Heaviside initial condition).

5 Quantization error of Greeks

Derivatives to the spatial variable are usually obtained from the finite difference approximation using difference formulas. In such usage, the quantization error retains the same form as the original finite difference approximation.

As an example, the quantization error propagates to the first central difference of the Heaviside approximation (3.22) as follows (up to second order in h):

$$\begin{aligned} E_{H\delta}^{(Q)}(x^*) &= \frac{ih}{2\pi}(\alpha - \frac{1}{2}) \int_{D_\zeta} e^{-ia\kappa - \kappa^2} e^{i\kappa x^*} \kappa d\kappa \\ & \quad - \frac{h^2}{4\pi}(\alpha^2 - \alpha + \frac{1}{6}) \int_{D_\zeta} e^{-ia\kappa - \kappa^2} e^{i\kappa x^*} \kappa^2 d\kappa. \end{aligned} \tag{5.1}$$

In other words, the grid positioning also gives rises to a first order error proportional to $(\alpha - \frac{1}{2})$ and the first derivative of a Gaussian centered at the discontinuity. Positioning the point of discontinuity at midpoint restores not only the second order error of the solution, but also that of the central first derivative as consistent with the theory for smooth functions.

6 Smoothing

Smoothing has long been a popular approach to obtain stable convergence and in some cases restore optimal order of convergence in the presence of non-smoothness in the initial data. In the financial context, a very popular approach is averaging ([8], [11], [4], [2]). This technique has been used successfully in the case of digital options (the initial condition being the Heaviside function). In this section, we will take a closer look at the smoothing technique in the context we developed in the earlier parts of the paper.

We start with the family of smoothing operators suggested in [5]. Their idea is to consider operators of the convolution type, which in frequency space corresponds to pointwise multiplication. In frequency space, define

$$\hat{\Phi}_\mu(h\kappa) = \frac{p_\mu(\sin \frac{h}{2}\kappa)}{(\frac{h}{2}\kappa)^\mu}, \tag{6.1}$$

where $p_\mu(\sin\omega)$ is a polynomial of degree μ in $\sin\omega$ that satisfies

$$p_\mu(\sin\omega) = \omega^\mu + O(\omega^{2\mu}), \quad \text{as } \omega \to 0.$$

The idea is that high frequency (large κ) components in the initial condition, which are often the cause for non-smoothness, can be damped simply by multiplication with $\hat{\Phi}_\mu$. The integer μ is considered the order of the smoothing operator, as, from the definition of p_μ we have

$$\hat{\Phi}_\mu(\omega) = 1 + O(\omega^\mu), \quad \text{as } \omega \to 0, \text{ and}$$

$$\hat{\Phi}_\mu(\omega) = O(|\omega - 2l\pi|^\mu), \text{as } \omega \to 2l\pi, l \in \mathbb{Z}.$$

The first two polynomials are particularly simple:

$$\begin{aligned} p_1(\sin\omega) &= \sin\omega \\ p_2(\sin\omega) &= \sin^2\omega. \end{aligned}$$

The first smoothing operator $\hat{\Phi}_1$ is the familiar averaging technique. To see this, it suffices to compute its inverse Fourier transform at a spatial point x:

$$\begin{aligned} \Phi_1(x) = \frac{1}{2\pi}\int_{-\infty}^{\infty} \frac{\sin\frac{h}{2}\kappa}{\frac{h}{2}\kappa} e^{i\kappa x} d\kappa &= \frac{1}{2\pi}\int_{-\infty}^{\infty} \frac{e^{i\frac{h}{2}\kappa} - e^{-i\frac{h}{2}\kappa}}{ih\kappa} e^{i\kappa x} d\kappa \\ &= \frac{1}{2\pi h}\int_{-\infty}^{\infty} \frac{e^{i\kappa(\frac{h}{2}+x)} - e^{i\kappa(-\frac{h}{2}+x)}}{i\kappa} d\kappa \\ &= \begin{cases} 0 & \text{if } |x| > \frac{h}{2} \\ \frac{1}{h} & \text{if } |x| < \frac{h}{2}. \end{cases} \end{aligned}$$

As a result, the convolution operator that $\hat{\Phi}_1$ induces in the spatial domain is of the form

$$(\Phi_1 * v)(x) = \frac{1}{h}\int_{-\frac{h}{2}}^{\frac{h}{2}} v(x-y)dy. \tag{6.2}$$

Similarly, the inverse transform of $\hat{\Phi}_2$ is

$$\Phi_2(x) = \begin{cases} 0 & \text{if } |x| > h \\ \frac{1}{h}\left(1 - \frac{|x|}{h}\right) & \text{if } |x| < h. \end{cases}$$

In convolution form, the second order smoothing takes the form

$$(\Phi_2 * v)(x) = \frac{1}{h}\int_{-h}^{h} (1 - \frac{|y|}{h}) v(x-y)dy. \tag{6.3}$$

We shall apply these operators to the initial conditions we have studied in Sections 3.2 through 3.4 and analyze how errors are affected by these techniques.

6.1 Dirac-delta function

As the Dirac-delta function is a generalized function, it can only be approximated on our numerical grid $x_j = (j + (1-\alpha))h$. If we replace formally the Dirac-delta function by the first order smoothed version of it (6.2), then we obtain the following approximation of the Dirac-delta initial condition (we leave out the case $\alpha = 0.5$ to avoid ambiguity):

$$v^{(0)}_{\Phi_1,\delta}(x_j) = \begin{cases} \frac{1}{h} & \text{if } \alpha < 0.5 \text{ and } j = -1 \\ \frac{1}{h} & \text{if } \alpha > 0.5 \text{ and } j = 0 \\ 0 & \text{else.} \end{cases}$$

Its discrete-time Fourier transform is

$$\hat{v}^{(0)}_{\Phi_1,\delta,\alpha,h}(h\kappa) = \begin{cases} e^{i\alpha h\kappa} & \text{if } \alpha < 0.5 \\ e^{-i(1-\alpha)h\kappa} & \text{if } \alpha > 0.5. \end{cases}$$

Clearly then

$$\hat{v}^{(0)}_{\Phi_1,\delta,\alpha,h}(h\kappa) = \begin{cases} 1 + i\alpha h\kappa + O(h^2) & \text{if } \alpha < 0.5 \\ 1 - i(1-\alpha)h\kappa + O(h^2) & \text{if } \alpha > 0.5. \end{cases}$$

In other words, had we started our analysis with this approximation of the Dirac-delta function, then we will end up with a first order error of our finite difference solution.

In fact, one can show that (3.5) is in fact the second order smoothing operator (6.3) applied formally to the Dirac-delta function. The results in Section 3.2 show that only the second order error term will remain, although the second order error depends quadratically on the relative position of the singularity on the grid.

6.2 Heaviside function

Applying (6.2) to the Heaviside function, we obtain the following modified initial condition:

$$v^{(0)}_{\Phi_1,H}(x_j) = \begin{cases} \frac{1-2\alpha}{2} & \text{if } \alpha < 0.5 \text{ and } j = -1 \\ \frac{3-2\alpha}{2} & \text{if } \alpha \geq 0.5 \text{ and } j = 0 \\ v^{(0)}_H(x_j) & \text{else.} \end{cases}$$

In other words, first order smoothing involves modifying only one point of the sampled function given any α. When $\alpha = 0.5$, the function is identical to the original sample of the unsmoothed Heaviside function $v^{(0)}_H(x_j)$. It is not surprising that the smoothing technique restores an error of second order in h. In fact, its discrete-time Fourier transform (for κ suitably defined on the complex plane) is

$$\hat{v}^{(0)}_{\Phi_1,H}(h\kappa) = \begin{cases} \tilde{v}^{(0)}_H(\kappa) + ih^2\kappa(-\frac{\alpha^2}{2} + \frac{1}{12}) + O(h^3) & \text{if } \alpha < 0.5 \\ \tilde{v}^{(0)}_H(\kappa) + ih^2\kappa(-\frac{\alpha^2}{2} + \alpha - \frac{5}{12}) + O(h^3) & \text{if } \alpha \geq 0.5. \end{cases}$$

The first order term, proportional to $(\alpha - \frac{1}{2})$ in (3.20) is removed by the first order smoothing technique. This observation has been noted in [8] and [11].

Although the first order error is successfully removed by smoothing, it is interesting to see what effect the second order smoothing operator Φ_2 would have on the Heaviside function. After applying (6.3) to the Heaviside function $v^{(0)}_H(x)$, one obtains

$$v^{(0)}_{\Phi_2,H}(x_j) = \begin{cases} \frac{(1-\alpha)^2}{2} & \text{if } j = -1 \\ \frac{2-\alpha^2}{2} & \text{if } j = 0 \\ v^{(0)}_H(x_j) & \text{else.} \end{cases}$$

Namely, the second order smoothing modifies two points on the sampled function. Its discrete-time Fourier transform is given by

$$\hat{v}^{(0)}_{\Phi_2,H}(h\kappa) = \tilde{v}^{(0)}_H(\kappa) + \frac{i\kappa h^2}{12} + O(h^3).$$

Therefore, the second order smoothing not only removes the first order error that would be present with a non-smooth Heaviside initial condition, it also removes the dependence of the second order error on α. The relative position of the grid no longer affects the dominant error term.

6.3 Call and put

The first order smoothing of the call and put gives the following modifications, respectively:

$$v^{(0)}_{\Phi_1,C}(x_j) = \begin{cases} \frac{(1-2\alpha)^2 h}{8} & \text{if } \alpha < 0.5 \text{ and } j = -1 \\ \frac{(3-2\alpha)^2 h}{8} & \text{if } \alpha \geq 0.5 \text{ and } j = 0 \\ v^{(0)}_C(x_j) & \text{else,} \end{cases}$$

$$v^{(0)}_{\Phi_1,P}(x_j) = \begin{cases} \frac{(1+2\alpha)^2 h}{8} & \text{if } \alpha < 0.5 \text{ and } j = -1 \\ \frac{(1-2\alpha)^2 h}{8} & \text{if } \alpha \geq 0.5 \text{ and } j = 0 \\ v^{(0)}_P(x_j) & \text{else.} \end{cases}$$

Type of initial condition	Unsmoothed	Φ_1 smoothing	Φ_2 smoothing
Dirac-delta	Not applicable	$O(h)$ error	$O(h^2)$ error, dependent on α
Heaviside	$O(h)$ error	$O(h^2)$ error, dependent on α	$O(h^2)$ error, independent of α
Usual Call, Put and Exponential Call, Put	$O(h^2)$ error, dependent on α	$O(h^2)$ error, independent of α	–

Table 6.1: Summary of the effect of smoothing techniques on CN-Rannacher error under different types of non-smooth initial conditions.

For κ suitably defined, the discrete-time Fourier transforms give

$$\hat{v}^{(0)}_{\Phi_1,C}(h\kappa) = \tilde{v}^{(0)}_C(\kappa) + \frac{h^2}{24} + O(h^3), \quad \text{and}$$

$$\hat{v}^{(0)}_{\Phi_1,P}(h\kappa) = \tilde{v}^{(0)}_P(\kappa) + \frac{h^2}{24} + O(h^3).$$

As a result, the first order smoothing successfully removes the dependence on α in the second order error. Removing the dependence on α is favorable, as the only computational parameters that affect the error will be step-sizes. This can be found convenient in some implementations. We summarize these discussions in Table 6.1.

7 Conclusions

In this paper, we have carried out a detailed investigation of the relationship between the numerical approximation error and the placement of the point of non-smoothness relative to the numerical grid (α), when solving the one-dimensional convection-diffusion equation with non-smooth initial conditions.

Our analysis has explicitly demonstrated the often non-linear relationship between α and the so-called *quantization error*, which arises from the non-smoothness of the initial condition. In addition, we have studied the possibility of an optimal choice of α. Based on a careful study of the quantization error, we also gave an example of a third order convergent numerical approximation despite using a formally second order scheme, due to a good choice of α. Moreover, using the quantization error formulae developed for the solution function, we derived such formulae for the Greeks, which are important hedging parameters. Finally, we demonstrate how smoothing operators not only recover the optimal order of convergence, as was proved in [5], but also remove the dependence of the leading discretization error on the placement parameter α. This could be a useful result for developing black-box numerical software that makes use of extrapolation techniques. In Table 7.1, we summarize our conclusions, in the form of recommendations to the user, as to when maintaining α and smoothing should be used alternatively or simultaneously, to preserve second and stable order of convergence.

It would be interesting to extend our analysis to higher order finite difference methods or to finite element methods. We also plan to extend our analysis to higher dimensional problems.

References

[1] R. Carter and M. B. Giles, *Sharp error estimates for discretizations of the 1D convection-diffusion equation with Dirac initial data*, IMA J. Numer. Anal., 27 (2007), pp. 406–425.

Initial condition	Second order error	"Stable" convergence
Dirac-delta type	Second order smoothing	Second order smoothing, and maintain α
Heaviside type	Placement at midpoint, or first order smoothing	Second order smoothing, or maintain α
Usual Call, Put and Exponential Call, Put type	–	First order smoothing, or maintain α

Table 7.1: Summary of recommendations on how to obtain second order error and stable convergence with non-smooth initial conditions, when CN-Rannacher method is used.

[2] D. Duffy, *Finite Difference Methods in Financial Engineering: A Partial Differential Equation Approach*, The Wiley Finance Series, Wiley, 2006.

[3] B. Dupire, *Pricing with a smile*, Risk, 7 (1994), pp. 18–20.

[4] S. Heston and G. Zhou, *On the rate of convergence of discrete-time contingent claims*, Math. Finance, 10 (2000), pp. 53–75.

[5] H. O. Kreiss, V. Thomée, and O. Widlund, *Smoothing of initial data and rates of convergence for parabolic difference equations*, Commun. Pure Appl. Math., 23 (1970), pp. 241–259.

[6] R. W. Lee, *Option pricing by transform methods: extensions, unification and error control*, J. Comput. Finance, 7 (2004), pp. 51–86.

[7] S. Mashayekhi and J. Hugger, *Kα-shifting, Rannacher time stepping and mesh grading in Crank-Nicolson FDM for Black-Scholes option pricing*, Commun. Math. Finance, 5 (2016), pp. 1–31.

[8] D. M. Pooley, K. R. Vetzal, and P. A. Forsyth, *Convergence remedies for non-smooth payoffs in option pricing*, J. Comput. Finance, 6 (2003), pp. 25–40.

[9] R. Rannacher, *Finite element solution of diffusion problems with irregular data*, Numer. Math., 43 (1984), pp. 309–327.

[10] C. Reisinger and A. Whitley, *The impact of a natural time change on the convergence of the Crank-Nicolson scheme*, IMA J. Numer. Anal., 34 (2014), pp. 1156–1192.

[11] D. Tavella and C. Randall, *Pricing Financial Instruments: The Finite Difference Method*, John Wiley & Sons, Inc., 2000.

[12] V. Thomée and L. Wahlbin, *Convergence rates of parabolic difference schemes for non-smooth data*, Math. Comput., 28 (1974), pp. 1–13.

[13] A.-K. Tornberg and B. Engquist, *Regularization techniques for numerical approximation of PDEs with singularities*, J. Sci. Comput., 19 (2003), pp. 527–552.

[14] A.-K. Tornberg and B. Engquist, *Numerical approximations of singular source terms in differential equations*, J. Comput. Phys., 200 (2004), pp. 462–488.

[15] J. D. Towers, *Finite difference methods for approximating Heaviside functions*, J. Comput. Phys., 228 (2009), pp. 3478–3489.

[16] H. WINDCLIFF, P. A. FORSYTH, AND K. R. VETZAL, *Shout options: a framework for pricing contracts which can be modified by the investor*, J. Comput. Appl. Math., 134 (2001), pp. 213–241.

[17] M. WYNS, *Convergence analysis of the Modified Craig-Sneyd scheme for two-dimensional convection-diffusion equations with nonsmooth initial data*, IMA J. Numer. Anal., 37 (2017), pp. 798–831.